# Pore network simulations of thin porous medium characterization by evapoporometry

Otman Maalal, Marc Prat, Didier Lasseux

International Journal of Multiphase Flow 167 (2023) 104547

DOI: 10.1016/j.ijmultiphaseflow.2023.104547

# Pore network simulations of thin porous medium characterization by evapoporometry

Otman Maalal [a,b], Marc Prat [a,], Didier Lasseux [b]

[a] Institut de Mécanique des Fluides de Toulouse (IMFT), Université de Toulouse, CNRS, Toulouse, France
[b] I2M, UMR 5295, CNRS, Univ. Bordeaux – Esplanade des Arts et Métiers, 33405 Talence, CEDEX, France

*Keywords:*
Pore body size distribution
Pore throat size distribution
Porous medium characterization
Pore network model
Numerical simulation

A B S T R A C T

Evapoporometry is a technique aiming at characterizing the pore size distribution of a porous medium from evaporated mass measurements. In this work, evapoporometry is studied from numerical simulations on model pore networks allowing a detailed analysis of the underlying physics at play in the technique. Simulations indicate that both the pore body size and throat size distributions can be characterized and pinpoint the need of a very accurate determination of the evaporation rate. This is notably illustrated by varying the evaporated mass acquisition time step. Evapoporometry and liquid-liquid displacement porometry techniques are discussed comparatively in relation with experimental works reporting differences between the pore size distributions identified through both techniques.

## 1. Introduction

The pore size distribution (PSD) is one of the most important characteristics of porous media and many experimental methods aiming at its determination have been developed, as reviewed in (Krantz et al., 2013; Tanis-Kanbur et al., 2019b). Typically, direct and indirect methods are commonly distinguished. Direct methods include microscopy and spectroscopic techniques, whereas measured quantities are used in indirect methods in order to determine the PSD on the basis of physical modeling employing for instance the Young-Laplace equation or the Kelvin equation. An advantage of the latter lies in their simplicity and in the fact that they generally do not require expensive dedicated equipment. Also, they allow characterizing larger and thus more representative portions of a porous medium. However, since the extraction of the pore sizes relies on theoretical considerations together with the use of a model, the quality and accuracy of the resulting identification is necessarily highly dependent on the relevance of the model. As a simple illustrative example, the extraction of the PSD in the Liquid-Liquid Displacement Porosimetry (LLDP) technique (Morrison, 2008; Peinador et al., 2010; Calvo et al., 2015) is commonly performed from the consideration of a model of cylindrical tubes in parallel. While the pore space geometry of some porous media, such as the Anopore$^{TM}$ membrane discussed in (Krantz et al., 2013), is reasonably close to a system of straight tubes in parallel, the situation for other porous media, such as PVDF membranes also illustrated in (Krantz et al., 2013), can be markedly different. The latter have an irregular fibrous, highly interconnected, porous structure. The question then arises as to whether the LLDP PSD extraction from the consideration of a bundle of straight tubes in parallel is still valuable when the pore space is highly interconnected. In the case of the LLDP, this question has been explored in previous works (Mourhatch et al., 2011; Maalal et al., 2021a; Maalal et al., 2022) where it was shown that serious errors on the PSD determination could be expected due to the connectivity of the pores. The LLPD example hence shows that it is important to elucidate what is really obtained from indirect methods. As for the LLPD, some clarification in this regard is of major interest for another indirect method, namely, the evapoporometry (EP) technique (Krantz et al., 2013; Tanis-Kanbur et al., 2019b). This is the purpose of the present study that is carried out by making use of numerical simulations. The EP technique is based on the measurement of the evaporated mass of a wetting liquid initially saturating the porous medium as a function of time, taking into account the dependence of the equilibrium vapor pressure with the meniscus curvature as described by the Kelvin relationship (Mitropoulos, 2008). In fact, two main EP techniques can be distinguished. In (Tanis-Kanbur et al., 2019b), the original technique presented in (Krantz et al., 2013) is modified in order to exclude the dead-end pores from the identified PSD. This implies the use of a non-volatile liquid in conjunction with the volatile liquid (see (Tanis-Kanbur et al., 2019b) for the details). In what follows, the original version of the method is considered. A common

**Nomenclature**

*Latin symbols*

| | |
|---|---|
| $A$ | Cross sectional area of the diffusion cell [$m^2$] |
| $a$ | Network lattice spacing [m] |
| $D_{eff}$ | Effective diffusion coefficient [$m^2.s^{-1}$] |
| $f$ | Probability density function [$m^{-1}$] |
| $k$ | Mass transfer coefficient [$m.s^{-1}$] |
| $L$ | Network length [m] |
| $l$ | Pore throat length [m] |
| $M_v$ | Molecular weight [$kg/mol^{-1}$] |
| $m$ | Mass of liquid in the porous structure [kg] |
| $P$ | Pressure [Pa] |
| $P_v$ | Vapor pressure [Pa] |
| $P_{vequ}$ | Equilibrium vapor pressure [Pa] |
| $P_{vsat}$ | Saturation vapor pressure [Pa] |
| $R$ | Ideal gas constant (8.314 [$J.mol^{-1}.K^{-1}$]) |
| $r$ | Pore, throat or tube radius [m] |
| $r_{curv}$ | Meniscus radius of curvature [m] |
| $r_{max}$ | Maximum expected pore radius [m] |
| $r_{min}$ | Minimum expected throat radius [m] |
| $r_t$ | Throat radius [m] |
| $S_p$ | Saturation in a pore body [-] |
| $S_t$ | Saturation in a pore throat [-] |
| $T$ | Temperature [K] |
| $t$ | Time [s] |
| $W$ | Evaporation rate [$kg.s^{-1}$] |
| $W_{ref}$ | Reference evaporation rate [$kg.s^{-1}$] |

*Greek symbols*

| | |
|---|---|
| $\Delta$ | Difference operator [-] |
| $\gamma$ | Interfacial tension [$N.m^{-1}$] |
| $\mu$ | Dynamic viscosity [Pa.s] |
| $\rho$ | Liquid density [$kg.m^{-3}$] |
| $\phi$ | Diffusive mass flow rate [$kg.s^{-1}$] |

*Superscript and subscript*

| | |
|---|---|
| $i, j$ | Element (pore body or throat) or time step index |

feature to both versions is to use menisci to probe the pore space, keeping in mind that the situation can be more or less complex depending on the structure of the porous medium. For instance, corrections must be introduced when the porous medium is asymmetric as discussed in (Krantz et al., 2013). Asymmetric in (Krantz et al., 2013) means, for instance, smaller pores in the upper region of the porous medium in contact with the evaporating atmosphere and larger pores beneath. In what follows, the idea is to consider the presumably simpler case of a homogeneous porous medium, which means that the probability of finding a pore of a given size is independent of the position of the pore within the porous layer. The original EP method consists in saturating the porous medium by a volatile wetting liquid, isopropanol being a commonly used fluid. As sketched in Fig. 1, the saturated thin porous medium is confined in a cylindrical diffusion test cell. The latter is placed on an electronic microbalance placed on an anti-vibration table (Krantz et al., 2013; Tanis-Kanbur et al., 2019b). The evaporated mass is recorded with the microbalance at a fixed time frequency (for instance every 10 s in the measurements reported in (Krantz et al., 2013)). The whole equipment is placed in an environmental chamber at a fixed temperature.

Initially, a liquid layer is present covering the upper surface of the saturated porous medium. This allows determining a reference evaporation rate independent of the throat size. After a while, once this liquid film is fully evaporated, evaporation of the liquid saturating the porous medium starts. Then the description of what happens differs in the

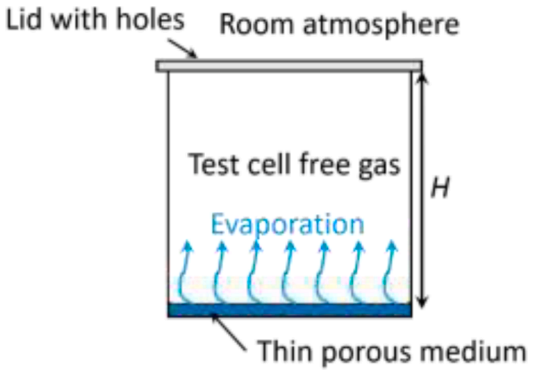


**Fig. 1.** Sketch of an evapoporometry test cell. Scales are distorted for clarity (the porous medium thickness is actually much smaller than the height, $H$, of the gaseous diffusion region in the test cell).

literature depending on the reference. In (Krantz et al., 2013), it is stated that "evaporation will progress from the largest to the smallest pores". In (Tanis-Kanbur et al., 2019a), it is written "the evaporation from a **saturated** membrane naturally occurs progressively from the largest pores to the smallest pores". This seems to suggest that the membrane remains saturated. On the other hand, it is written in (Krantz et al., 2013), "all the pores smaller than those draining", which is a clear indication that pores empty. This is in full agreement with our model in Section 3.2, which explicitly compute the gradual invasion of the pore space by the gas phase as a result of evaporation. In this respect, it seems that there is a major difference between the original reference (Krantz et al., 2013), where the liquid in pores drain, and the description of the EP technique in (Tanis-Kanbur et al., 2019a), where it is explicitly stated that "the PSD can be quantified by measuring the evaporation rate from the saturated membrane...". Clarifying this issue is important because one may argue that the menisci never retreat into the pores and, further, that the pores at the surface are always filled with liquid. In our opinion, this is a major misconception of the evaporation process taking place while carrying out EP, at least for the symmetrical porous medium considered in the present study. For us, in agreement with (Krantz et al., 2013), the gas phase gradually invades the pore space and the resulting receding menisci are the probes allowing to determine the pore sizes. As a matter of fact, it is also an objective of this work to clarify the underlying physics in the EP technique.

To this end, the present study is based on pore-scale modelling and numerical simulations of the processes occurring in the EP technique. The advantage of the numerical procedure developed here is that the PSD is perfectly known a priori for the model pore structure under consideration since this is an input of the model. This PSD is referred to as the reference PSD. The evaporation process occurring in the EP is numerically simulated in the model pore structure. From these simulations, corresponding quantities measured in the EP technique, namely the evaporated mass and evaporation rate, are computed and the PSD is extracted using interpretation procedures commonly used in EP. Finally, the resulting PSDs are compared to the reference PSDs. The two-phase flow simulations with evaporation (EP) in the model porous medium is performed using a technique called pore network modelling (PNM), (see *e.g.* Blunt, 2001; Blunt et al., 2002). As discussed in Maalal et al. (2021a), this technique is based on the representation of the pore space as a network of two main types of structural elements: the pore bodies and the pore throats. As schematically illustrated in Fig. 2, the pore bodies correspond to the local larger volumes in the pore space, whereas the pore throats correspond to the constrictions, that is, to the narrower

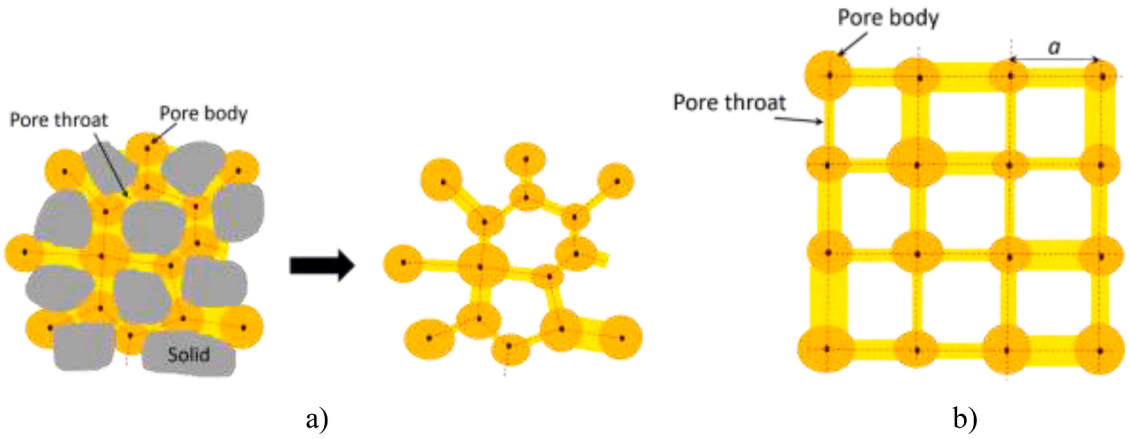


**Fig. 2.** (a) Schematic partition of the pore space in pore bodies (shown in orange) and pore throats (in yellow) and extracted pore network; (b) square (2D) model pore network (the black dots correspond to the computational nodes).

passages between the pore bodies. The concept of pore network is illustrated in Fig. 2a. In Fig. 2b, the simplified pore network considered for the present study is sketched. It consists of a square pore network where the pore bodies are spheres located at the nodes of a regular square grid whereas the pore throats are narrower cylindrical channels between pore bodies.

This pore space partition leads to the consideration of two main distributions for characterizing the pore space: the pore body size distribution (PBSD) and the pore throat size distribution (PTSD). The latter is simply denoted by TSD in the following. Hence, the distinction is made in this study between the TSD and the PBSD. To assess the TSD and PBSD extraction from EP simulations, the paper is organized as follows. In section 2, the physical characteristics of interest involved in EP are briefly presented. The model porous medium, a simple square pore network, is presented in Section 3 together with the EP evaporation PNM algorithms. Simulation results are presented in Section 4. A short discussion is presented in Section 5. Conclusions are drawn in Section 6.

## 2. Evapoporometry (EP)

The invasion of the pore space by menisci affects the evaporation rate because the (isopropanol) equilibrium vapor pressure, $P_{vequ}$, at the surface of a curved meniscus depends on the meniscus curvature. This effect is quantified thanks to Kelvin's relationship (Mitropoulos, 2008), which for a meniscus in a cylindrical pore is expressed as,

$$P_{vequ} = P_{vsat}\exp\left(-\frac{M_v}{RT}\frac{2\gamma}{\rho r_{curv}}\right) \tag{1}$$

where $P_{vsat}$ is the saturation vapor pressure at the temperature, $T$, of the ambient atmosphere, $M_v$ is the volatile liquid molecular weight, $R$ is the universal gas constant, $\rho$ is the liquid density and $r_{curv}$ is the meniscus radius of curvature.

Note that the height, $H$, of the test cell (Fig. 1) is much larger than the porous medium thickness. For instance, $H = 10.5$ cm in the set-up used in (Krantz et al., 2013) and 2.5 cm in the one used in (Tanis-Kanbur et al., 2019a). Since the porous medium thickness is small compared to the diffusion length, $H$, in the cell, it is assumed that the external mass transfer is essentially in the direction orthogonal to the porous medium surface, between the top surface of the porous medium and the top of the cell. By contrast, the internal mass transfer refers to the mass transfer inside the porous medium pore space. The evaporation rate is thus expressed as,

$$W \approx kA\frac{M_v}{RT}P_{vequ} \tag{2}$$

where $P_{vequ}$ is the equilibrium vapor pressure corresponding to a mean radius, $r_{curv}$, of the menisci exposed to evaporation at the time at which $W$ is observed. Here, $A$ is the cross-sectional area of the diffusion cell and $k$ is the external mass transfer coefficient. The latter can be determined from the evaporation rate when the liquid film is present

$$W_{ref} \approx kA\frac{M_v}{RT}P_{vsat} \tag{3}$$

Note that the isopropanol vapor partial pressure at the top of the cell is very small and considered in practice to be equal to zero. Combining Eqs. (2) and (3) yields

$$\frac{P_{vequ}}{P_{vsat}} = \frac{W}{W_{ref}} \tag{4}$$

When this result is introduced in the Kelvin relationship, Eq. (1), the average meniscus radius of curvature can be expressed as a function of the evaporation rate as

$$r_{curv} = -\frac{M_v}{RT}\frac{2\gamma}{\rho\ln\left(\frac{W}{W_{ref}}\right)} \tag{5}$$

The evaporation rate is determined from the evaporated mass measurement. Consider two successive measurements of the liquid mass, $m_i$ and $m_{i+1}$, corresponding to two times, $t_i$ and $t_{i+1}$. The evaporation rate is then simply computed as,

$$W = \frac{m_{i+1} - m_i}{t_{i+1} - t_i} \tag{6}$$

In the EP technique, it is admitted that the radius of curvature of a meniscus is close to the element (pore body or throat) radius, $r$, in which the meniscus is located, in accordance with the hypothesis of a perfectly wetting liquid, thus $r_{curv} \approx r$. Assuming that during the interval $t_{i+1} - t_i$, the fraction of liquid only contained in elements (pore bodies or throats) of radius $r$ was evaporated, the corresponding mass fraction, $f_{EP}$, is simply given by

$$f_{EP} = \frac{m_{i+1} - m_i}{m_t} \tag{7}$$

where $m_t$ is the total mass of liquid initially filling the porous medium. The PSD, or more precisely the PBTSD (where PB stands for pore bodies and T for throats) is actually obtained in a discrete form. The distribution interval $[r_{min}, r_{max}]$ is divided into $n_b$ bins, $r_{min}$ and $r_{max}$ being respectively the minimum and maximum element radius present in the porous medium. A radius is evaluated corresponding to each time interval of the experimental mass evaporation rate curve using Eqs. (2) and (5) and the associated fraction, $f_{EP}$, is determined from Eq. (7). The cumulative mass fractions corresponding to each radius contained within each bin hence leads to the determination of the fraction of

elements of this bin, finally leading to the PBTSD discretized in $n_b$ intervals.

In Fig. 3, the variation of the equilibrium vapor pressure is represented as a function of the meniscus radius of curvature for isopropanol as determined from Eq. (1). The Kelvin effect is noticeable only for radii of curvature in the submicronic range, and more significantly for radii approximately below 20 - 25 nm. The EP technique is therefore suitable for porous media with sufficiently small pores, such as ultrafiltration membranes for example (Krantz et al., 2013), whose pores are typically in the range [1 - 100 nm]. However, for very small pores of radius below 2 nm, applicability of Kelvin's relationship can be questioned (Takei et al., 1997). Actually, the maximum pore size that can be identified depends on the precision of the scale used to measure the evaporated mass and the choice of the volatile liquid (Akhondi et al., 2015; Zamani et al., 2017) but the method cannot be extended, in practice, beyond a few hundreds of nanometers.

## 3. Pore network models

As previously stated, EP pore scale physical processes are simulated in the model pore structure depicted in Fig. 2b, using pore network models (PNM). The aim of the PNM is to simulate the evaporation process occurring during an experimental EP operation. To this end, the PNM algorithm described in (Maalal et al., 2021b) is used. A summary of this algorithm is given below. The network is fully saturated with liquid at the beginning of the simulations.

### 3.1. Pore network

As illustrated in Fig. 2b, the model pore structure considered in this study is a square network. Pore bodies, *i.e.*, the local larger cavities, are located at the nodes of the square grid. The network size is the number of pore bodies in the network along each main direction. Simulations are performed on 20 × 20 networks. The distance between the centers of two adjacent pore bodies is the lattice spacing $a$. In the present study, $a$ = 300 nm. The pore bodies are spheres of radius $r_p$. Pore body radii are distributed randomly within a specified range [$r_{pmin}$, $r_{pmax}$] according to a given probability density function (p.d.f.). Pore throats connecting the pore bodies are cylinders of radius $r_t$. The throat size is also randomly distributed within a specified range [$r_{tmin}$, $r_{tmax}$] according to a given p.d.f. with the constraint that a throat radius cannot be larger than the smallest radius of the two adjacent pore bodies radii. In this work, the pore body size distribution (PBSD) and throat size distribution (TSD) are either Gaussian or uniform. The length, $l$, of a throat is computed from the lattice spacing and the sizes of the neighboring pore bodies 1 and 2 as,

$$l = a - r_{p1} - r_{p2} \tag{8}$$

### 3.2. Evapoporometry pore network model

As discussed in (Maalal et al., 2021b) and illustrated in Fig. 4, the evaporation process is characterized by the formation of liquid clusters. In order to compute the evaporation rate from each cluster, the isopropanol vapor partial pressure at each node $i$ of the network occupied by the gas phase is determined from the mass balance,

$$\sum_h \varphi_{ij} = 0. \tag{9}$$

Here, $\phi_{ij}$ is the diffusive mass flow rate between pore bodies $i$ and $j$ if both are fully occupied by the gas phase or between pore body $i$ and the meniscus at the entrance of an adjacent throat if this throat is occupied by the liquid phase. The diffusive mass flow rate, $\phi_{ij}$, is computed using Fick's law. For instance, between two gaseous pore bodies connected by a gaseous throat, $\phi_{ij}$ reads

$$\phi_{ij} = D_{eff}\frac{M_v}{RT}\,\pi r_{tij}^2\left(\frac{P_{vj} - P_{vi}}{a}\right) \tag{10}$$

where the effective diffusion coefficient, $D_{eff}$, is computed as the harmonic mean of the vapor molecular diffusion coefficient and the Knudsen diffusion coefficient (Maalal et al., 2021b). To obtain the vapor partial pressure field from Eq. (9), boundary conditions must be specified. Here, zero flux conditions are imposed at the lateral and bottom sides of the network. The coupling with the external mass transport in the cell is performed by locating additional computational nodes in the test cell, *i.e.*, in the gas region of height $H$ above the porous medium represented in Fig. 1. In this purely gaseous layer, also referred to as the external gas layer, the diffusive mass flow rate, $\phi_{ij}$, between two nodes $i$ and $j$, reads $\phi_{ij} = D\frac{M_v}{RT}\,\pi a^2\left(\frac{P_{vj}-P_{vi}}{a}\right)$, where $D$ is the vapor molecular diffusion coefficient. The consideration of this external diffusive layer allows computing simultaneously the vapor partial pressure field in both the network and the external gas layer. A zero vapor partial pressure is

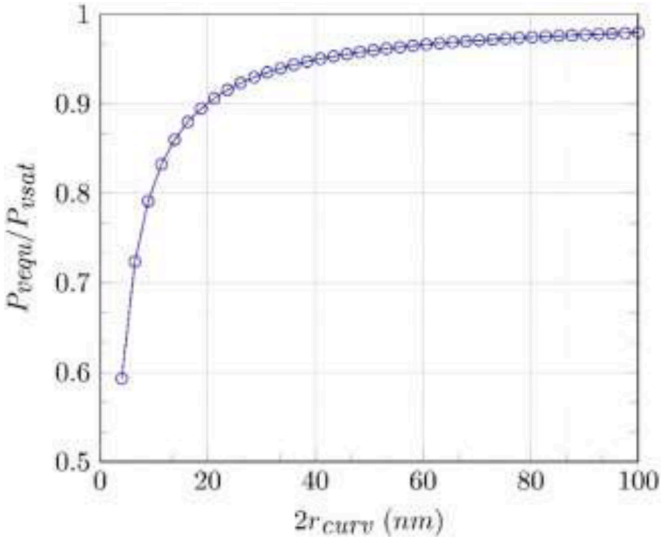


**Fig. 3.** Equilibrium vapor pressure as a function of meniscus radius of curvature for isopropanol.

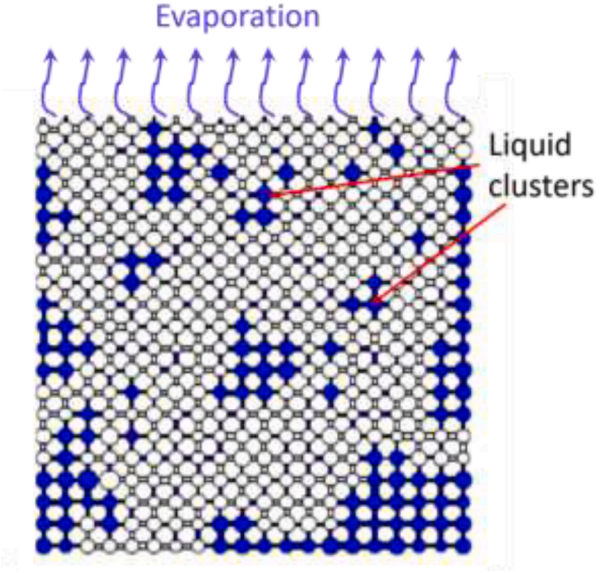


**Fig. 4.** EP fluid distribution in the network (liquid clusters in blue, gas phase and solid phase in white).

imposed on top of the external gas layer. One can refer to (Maalal et al., 2021b) for more details. Since a key feature of an EP test cell is that the porous medium thickness is much smaller than the cell height, an external layer of height $H$ equal to $500a$ is considered. The network to diffusion layer thicknesses ratio is thus equal to $\frac{20a}{500a} = 0.04$ in the simulations. It is about two orders of magnitude larger than in the set-up used in (Tanis-Kanbur, 2019a) where $H = 25$ mm and the porous medium active thickness is on the order of 10 μm. Nevertheless, this ratio can be reasonably considered as sufficiently small for the hypothesis of a unidirectional evaporation flux to be valid. A key issue is the specification of the vapor partial pressure at the boundary of each cluster, or, according to the Kelvin relationship given in Eq. (1), the radius of curvature of the menisci forming each liquid cluster boundary. First, on the grounds that the evaporation process is quite slow in the EP, as a result of the significant height $H$ of the test cell, viscous effects can be neglected and, therefore, the fluid distribution evolution in the network is controlled by capillary effects only. The consequence is that the radius of curvature is the same for every meniscus at the boundary of a given cluster. Second, it is argued that the meniscus curvature at the boundary of a given cluster should adapt so that the mass flow rate from a cluster cannot be negative. By convention, the mass flow rate from a cluster is positive when there is a net evaporation. A negative mass flow rate would correspond to condensation, thus to a potential growth of the cluster and, therefore, to a change in the meniscus radius of curvature. As explained in (Maalal et al., 2021b), an iterative numerical procedure, implying to solve repeatedly the system of equations obtained from Eq. (9), is used to determine the radius of curvature, that is, the isopropanol equilibrium vapor partial pressure at the boundary of each cluster so that there is no negative cluster mass flow rate. Once the iterative procedure reaches convergence, the evaporation rate, $\phi_i$, at the boundary of each cluster $i$ present in the network can be computed. Then the procedure is similar to that for drying PNM simulation in the absence of Kelvin effect (Prat, 1993). The evaporation algorithm in the presence of the Kelvin effect can finally be summarized as follows:

(1) All liquid clusters present in the network are labelled.
(2) The interfacial element (pore body or throat) with the lowest threshold capillary pressure, *i.e.*, of greatest size, is identified for each cluster; $m_{ci}$ is the mass of liquid present in this element for cluster $i$.
(3) The vapor partial pressure at the boundary of each cluster is computed employing the iterative procedure outlined above.
(4) The evaporation rate, $\phi_i$, at the boundary of each cluster is computed.
(5) For each cluster, the mass loss corresponding to the evaporation rate determined in step (4) is assigned to the element identified in step (2).
(6) The element eventually invaded is the one which is the first to be completely drained among the elements selected in step (2). This element is identified from the invasion time associated to each cluster given by $\delta t_{ci} = m_{ci}/\phi_i$ as the element of smallest $\delta t_{ci}$. This also defines the PNM time step as $\Delta t_{PNM} = \min(\delta t_{ci})$, which therefore varies during the drying simulation.
(7) The phase distribution within the network is updated and the procedure is iterated starting from step (1).

A typical fluid distribution obtained with the above algorithm and made of many liquid clusters is represented in Fig. 4. As discussed in (Prat, 1993), invasion percolation rules (Wilkinson & Willemsen, 1983) are used to model the drying process; this corresponds to step (2) in the above algorithm. This means that elements of larger size are preferentially invaded, which is perhaps not in exact agreement with the ambiguous statement in (Krantz et al., 2013) that evaporation progress from the largest to the smallest pores. In the evaporation process, the liquid in the emptying pores is drawn by capillary action into the smaller pores, which therefore are the last to dry. It is less ambiguous to state that the invasion of the pore space by the gas, as a result of evaporation, progresses from the largest to the smallest pores because evaporation can actually be negligible at a moving meniscus when this meniscus is located far enough from the top surface of the network. The flow driven by capillarity between larger interfacial pores and smaller ones is referred to as the capillary pumping effect. Here, interfacial means pore with a meniscus. This effect helps maintain liquid filled small pores at the surface of the porous medium during drying.

In direct link with the EP, the EP PNM allows computing the mass variation as a function of time due to evaporation as well as the evaporation rate $W$. The mass is simply obtained as

$$m(t) = m(0) - \rho \sum_{i=1}^{i=n_t} S_{ti}(t) V_{ti} - \rho \sum_{i=1}^{i=n_p} S_{pi}(t) V_{pi} \tag{11}$$

where $n_t$ and $n_p$ are respectively the number of throats and pore bodies in the network, $V_{ti}$ ($V_{pi}$, respectively) is the volume of throat (pore body, respectively) $i$, $S_{ti}$ ($S_{pi}$, respectively) is the saturation in the throat (pore body, respectively) $i$. The latter is equal to 1 when the element is fully occupied by the liquid, zero when the element is empty (that is fully occupied by the gas-phase) and between 0 and 1 when the element is partially filled with liquid.

The evaporation rate, $W_{PNM}$, is determined from the vapor partial pressure field by summing up all the mass flow rate contributions between two horizontal adjacent rows of computational nodes in the external boundary layer using expressions similar to Eq. (10)

$$W_{PNM}(t) = -\sum_{1}^{N} D_{eff} \frac{M_v}{RT} a^2 \left( \frac{P_{vj} - P_{vi}}{a} \right) \tag{12}$$

In this expression, $N$ is the number of computational nodes in the horizontal direction, $P_{vj}$ and $P_{vi}$ are the vapor partial pressures at the upper and lower rows of nodes between which the evaporation rate is computed. Then the element (pore bodies and throats) probability density function can be determined from

$$f_{EP-PNM} = \frac{W_{PNM}\left(\frac{t_i + t_{i-1}}{2}\right)(t_i - t_{i-1})}{m_t} \tag{13}$$

where $t_i$ and $t_{i-1}$ are two successive elapsed times in the EP PNM simulation.

The evaporation rate can be also computed as in the EP procedure (Eq. (6)) from

$$W_m\left(\frac{t_i + t_{i-1}}{2}\right) = \frac{m(t_i) - m(t_{i-1})}{t_i - t_{i-1}} \tag{14}$$

where $t_i$ and $t_{i-1}$ are two successive elapsed times. In principle, $W_{PNM}$ and $W_m$ must be equal but, as will be detailed below, the EP procedure can introduce some errors due to its discrete nature, more specifically because of the fact that the evaporation rate is determined at a fixed time frequency. For this reason, it is interesting to distinguish $W_{PNM}$ from $W_m$. Then the element (pore bodies and throats) probability density function is determined from the equivalent of Eq. (7), namely,

$$f_{EP-m} = \frac{m_{i+1} - m_i}{m_t} \tag{15}$$

The EP PNM simulations were performed for the isopropanol physical properties summarized in Table 1

## 4. Results

The EP PNM simulations were performed for a $20 \times 20$ network and two types of element distributions: uniform or Gaussian. Details on the distributions are given in Table 2. These distributions are the reference TSD and PBSD; they are depicted in Fig. 5.

In Fig. 6, the variation of the evaporation rate, as determined from

**Table 1**
Isopropanol physical properties and temperature condition

| | |
|---|---|
| Interfacial tension (N/m) | $2.17 \times 10^{-2}$ |
| Contact angle | 0 |
| Density (kg/m$^3$) | 786 |
| Molecular weight (kg/mol) | $6.1 \times 10^{-2}$ |
| Temperature (K) | 293 |
| Saturation vapor pressure (Pa) | 4400 |
| Binary diffusion coefficient (m$^2$/s) | $1.06 \times 10^{-5}$ |
| Dynamic viscosity (Pa.s) | $2.37 \times 10^{-3}$ |

**Table 2**
Reference uniform and Gaussian TSD and PBSD.

| p.d.f. type | Uniform | Gaussian |
|---|---|---|
| TSD | $r_{tmin} = 2$ nm, $r_{tmax} = 50$ nm | Mean: 25 nm<br>Standard deviation: 7 nm |
| PBSD | $r_{pmin} = 80$ nm, $r_{tmax} = 120$ nm | Mean: 100 nm<br>Standard deviation: 10 nm |

Eq. (12), is represented versus time for the uniform and Gaussian distributions. In this figure, $W_{PNM}(t)$ is normalized by the evaporation rate, $W_0$, at t = 0, *i.e.*, when the network is fully saturated and the menisci at the network surface are flat. One can observe a long plateau followed by an abrupt drop in the evaporation rate. At first glance, these curves look very similar to the ones reported in the EP experimental works, (Krantz et al., 2013; Tanis-Kanbur et al., 2019a). However, the interpretation is different here.

In (Krantz et al., 2013), the plateau is entirely attributed to the evaporation of the liquid film standing initially at the surface of the porous medium and the drop in the evaporation rate is attributed to the occurrence of evaporation in the pores. In (Tanis-Kanbur et al., 2019a), part of the plateau is attributed to the evaporation of the free-standing liquid initially present on the top of the membrane. In the present simulations, there is no film. Initially, the network is saturated and in contact with the test cell atmosphere at its top surface. Clearly, the plateau corresponds to evaporation in the pores. This is illustrated in Fig. 7, which shows the computed fluid distribution in the network at different times. This is an indication that excessive care must be taken while interpreting the experimental evaporation rate curve versus time as the constant rate period may include part of the evaporation within the pores, depending on the pore structure.

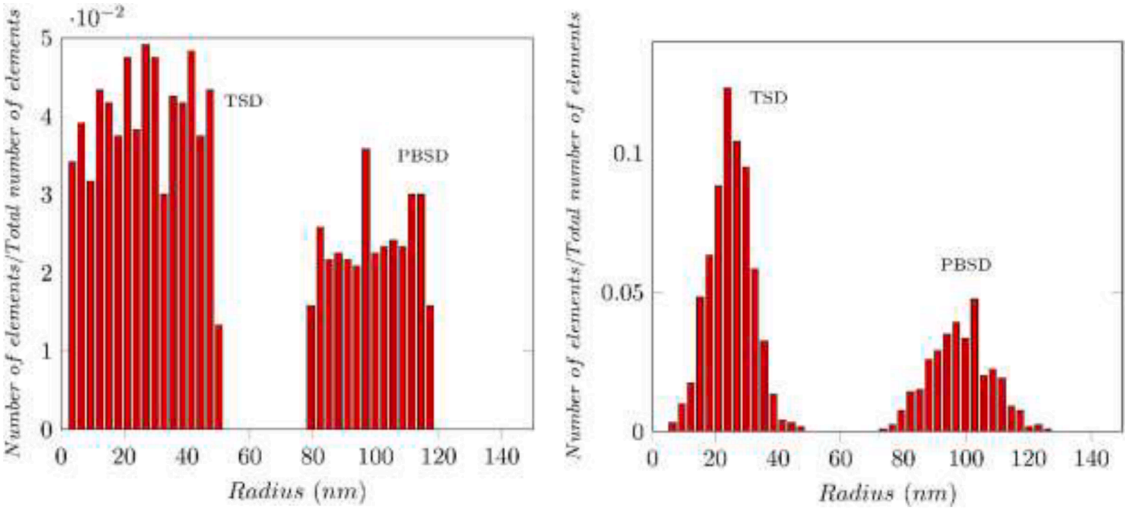


**Fig. 5.** Reference uniform (a) and Gaussian (b) TSD and PBSD.

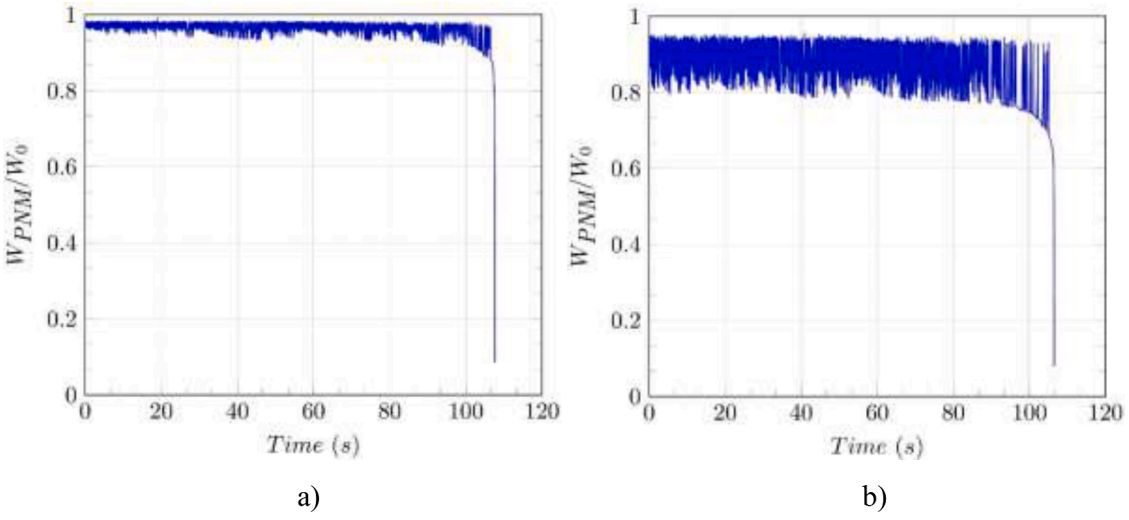


**Fig. 6.** Normalized evaporation rate as a function of time for the uniform (a) and Gaussian (b) TSD and PBSD.

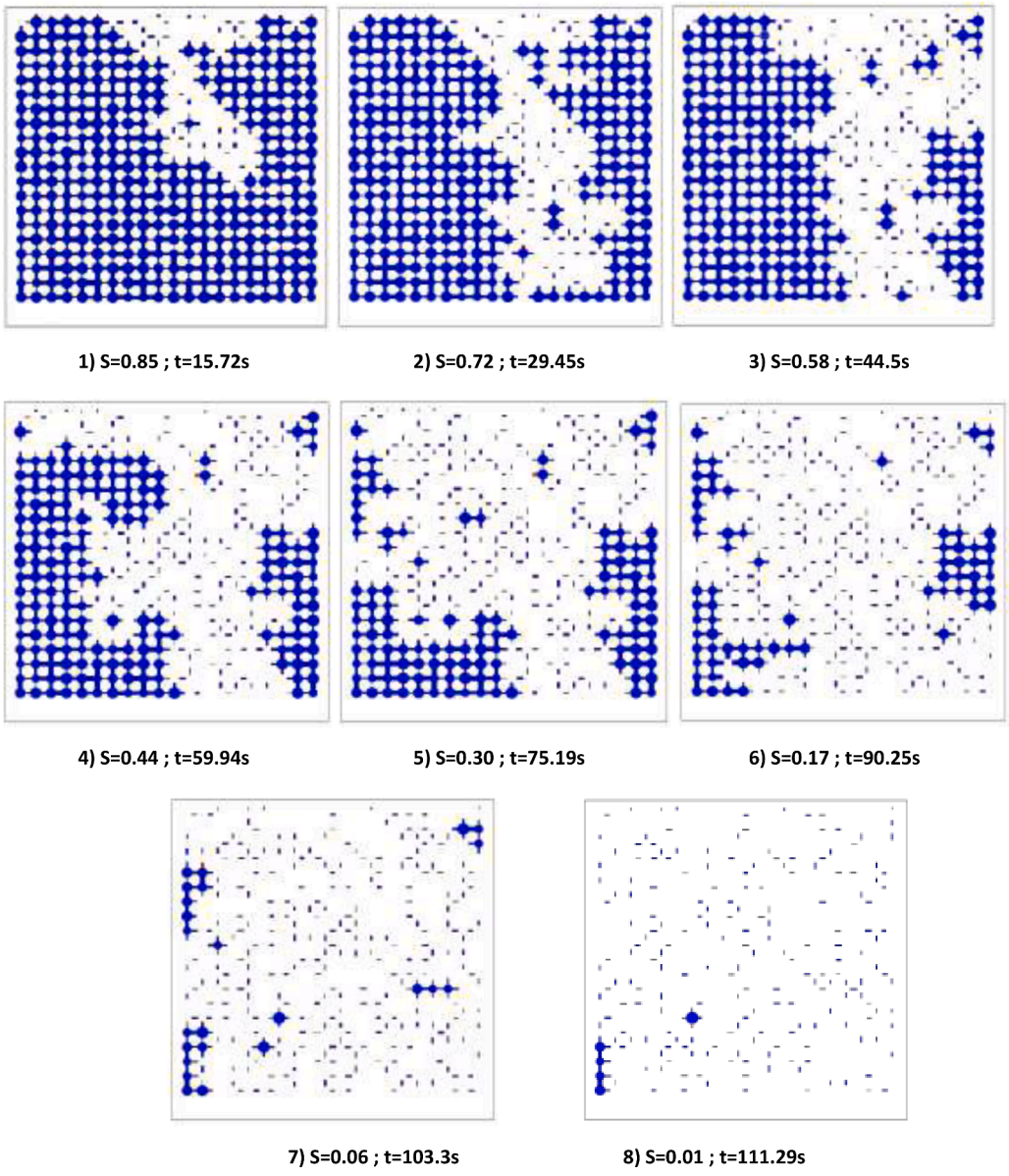


**Fig. 7.** Liquid (in blue) gas (in white) distributions in the network at different times for the case corresponding to Fig. 5a (uniform distributions).

It must also be noted that the evaporation rate obtained from the numerical simulations fluctuates with time. In other words, the evaporation rate can slightly increase during the drying process. This somewhat counter-intuitive result is due to the Kelvin effect. As discussed in (Maalal et al., 2021b), the vapor pressure at the boundary of each cluster fluctuates because of the menisci curvature fluctuations during the drying process. As a result, when, for instance, a larger throat becomes an interfacial throat, the menisci curvature decreases and therefore the menisci vapor pressure increases according to Kelvin's relationship. This, in turn, induces a larger evaporation rate. The origin of the fluctuations can be simply illustrated with the situation depicted in Fig. 8, assuming that the porous medium is made here, for simplicity, of a spatially periodic arrangement of non-interconnected vertical columns of cylindrical pores of variable section. Only the top of a single column of pores is shown in Fig. 8.

Since the size of pore A is smaller than that of pore B, $P_{veq.A}<P_{veq.B}$ according to Kelvin's relationship given in Eq. (1). Then, since the porous medium, and thus the distance between two pores, is very small compared to the length of the free gas region in the test cell, *i.e.*, $a<<H$, the evaporation rate, when the meniscus is in pore A, is $W_A \approx$

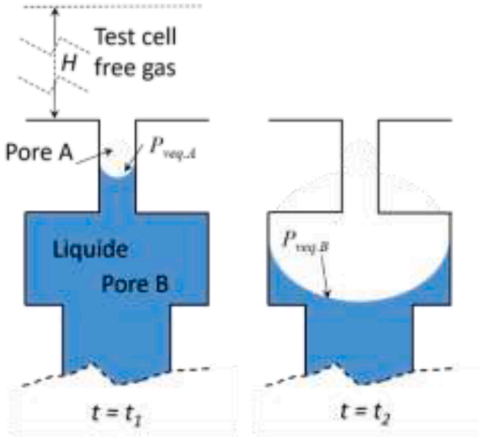


**Fig. 8.** Illustrative situation leading to an increase in the evaporation rate when the meniscus moves from pore A to pore B.

$kA\frac{M_v}{RT}P_{vequ\ A}$ and equal to $W_B \approx kA\frac{M_v}{RT}P_{vequ\ B}$ when the meniscus is in pore B. Since $P_{vequ\ A} < P_{vequ\ B}$, $W_B > W_A$. Thus, the evaporation rate increases when the meniscus moves from pore $A$ to pore $B$. Conversely, the evaporation rate may again decrease if the meniscus moves into a smaller pore below pore B.

As a consequence, the fluctuations, as illustrated in Fig. 6, should not be confused with possible parasitic fluctuations that might occur during mass measurement in the experimental EP operation. The fluctuations depicted in Fig. 6 are intrinsic to the drying process and it is important to capture them properly as discussed below.

The TSD and PBSD, obtained from the results shown in Fig. 6 and by applying Eq. (5), together with the expression of $W_{PNM}$ given in Eq. (12), are depicted in Fig. 9 and 10 for the reference uniform and Gaussian distributions, respectively.

As can be seen from Figs. 9 and 10, the results are quite appealing. Both element populations, namely the throats and the pore bodies, are retrieved. The sizes are in the correct ranges. In the case of the Gaussian distributions, the identified distributions are reasonably Gaussian-like. The identified and reference uniform distributions are also reasonably similar. However, it can be observed that the pore bodies and throats fractions are different in the extracted distributions compared to the reference ones. In brief, there are much less throats than pore bodies in the identified distributions compared to the reference distributions.

This difference may be explained as follows. The pore fractions presented in the distributions obtained with the evapoporometry procedure are weighted by the mass of each pore body or throat, that is, by the volume of each element. In other words, the probability densities obtained from the EP procedure represents the contribution of the throats or pore bodies to the volume of the pore space in the membrane. As the pore bodies have volumes greater than the throats (keeping in mind that the pore body sizes are greater than the adjacent throat sizes), the extracted probabilities of pore bodies are consequently greater in comparison with the throat ones. Therefore, to make a fair comparison, the reference TSD and PBSD should represent the volume fraction of the porous void as well, rather than simply the fraction of the number of elements. For every pore body or throat, the corresponding probability density function is the volume of that pore body (sphere) or throat (cylinder) divided by the total void volume. The reference TSD and PBSD obtained after this correction is applied are reported in Fig. 11a and 11b for the uniform and Gaussian distributions respectively.

As can be observed from the comparison between Figs. 9-10 and

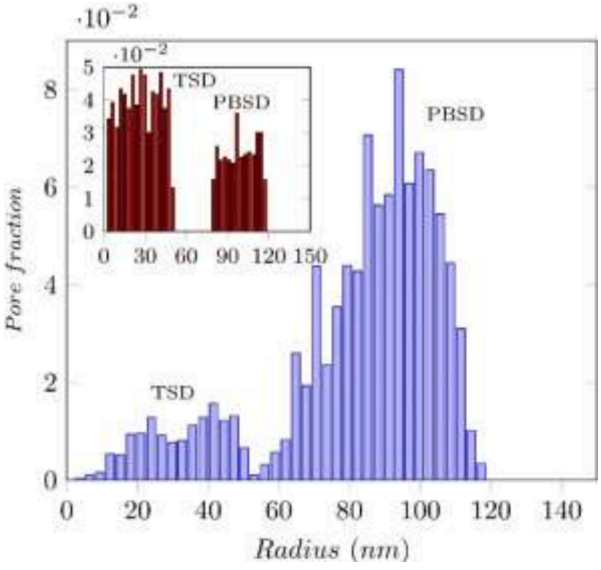


**Fig. 9.** TSD and PBSD obtained from EP using the $W_{PNM}$ curve (Fig. 6) for the uniform reference distributions (shown in the inset).

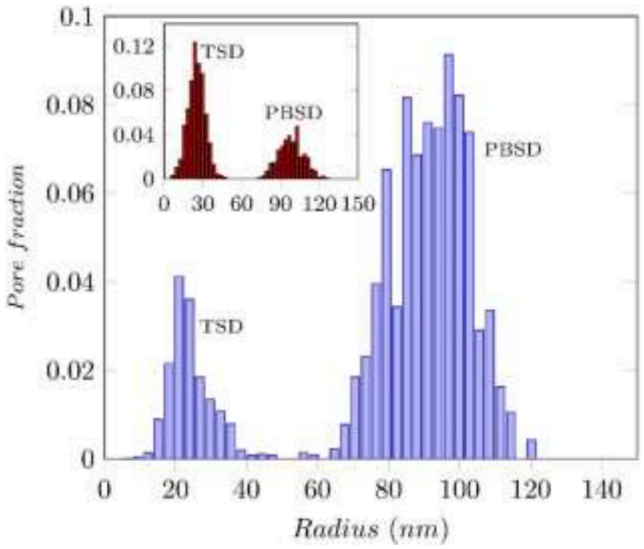


**Fig. 10.** TSD and PBSD obtained from EP using the $W_{PNM}$ curve (Fig. 6) for the Gaussian reference distributions (shown in the inset).

Fig. 11, the agreement between the extracted distributions (Figs. 9 and 10) and the reference distributions (Fig. 11) is quite satisfactory. The contribution of each element category, *i.e.*, pore bodies or throats, to the pore space volume is fairly well retrieved.

Clearly, these results are quite in favor of the EP technique for the identification of the pore and throat size distributions. However, it must be emphasized that the experimental EP procedure does not allow the direct measurement of the evaporation rate within the cell test in order to obtain the equivalent of $W_{PNM}$ in the simulations. In the experimental EP, the evaporation is actually deduced from the mass variation measurements by making use of Eq. (14). Furthermore, in the experimental procedure, the mass is measured at a fixed time frequency, whereas in the PNM simulations, the time step depends on the volumes of the throats or pore bodies emptying over the time step under consideration that is therefore variable. Moreover, $W_{PNM}$ is determined at a quite high frequency in the PNM simulation because it is determined at each time step, *i.e.*, each time an element (pore body or throat) gets completely empty in the network. This is illustrated in Fig. 12 which shows that the PNM time step typically varies in the range [0 - 0.3 s] in the simulation reported above. The varying time step, $\Delta t_{PNM}$, in the PNM simulation (defined in the PNM algorithm in section 3.3) is referred to as the intrinsic time step in what follows.

In order to make a more accurate assessment of the experimental procedure, simulations were carried out considering a constant time step $\Delta t$. This means that the liquid mass in the network was computed at constant intervals of time, $\Delta t$, and that the evaporation rate was computed from the resulting mass variation with time by making use of Eq. (14) in which $t_{i+1}-t_i=\Delta t$. The probability density function was extracted from Eq. (15). The element size at the elapsed time under consideration was then deduced from Eq. (5). This procedure was tested for three fixed time steps, namely $\Delta t = 0.005$ s, $\Delta t$=0.1 s, and $\Delta t = 1$ s in the case of the reference Gaussian distributions for both the pore bodies and throats. This leads to the results on the PBTSD reported in Fig. 13b-d. The result on the PBTSD, obtained when all the mass evolution information available from the simulation is employed, is represented in Fig. 13a, showing that, both the TSD and PSD are quite well retrieved (see Fig. 11b for comparison with the reference distribution) in that case.

When a sufficiently small fixed value of $\Delta t$ is employed, *i.e.*, on the order or less than the PNM time steps (Fig. 12), namely $\Delta t$=0.005 s, the procedure with a constant time step leads to quite good results. As illustrated in Fig. 13b, the TSD and PBSD obtained with this time-step

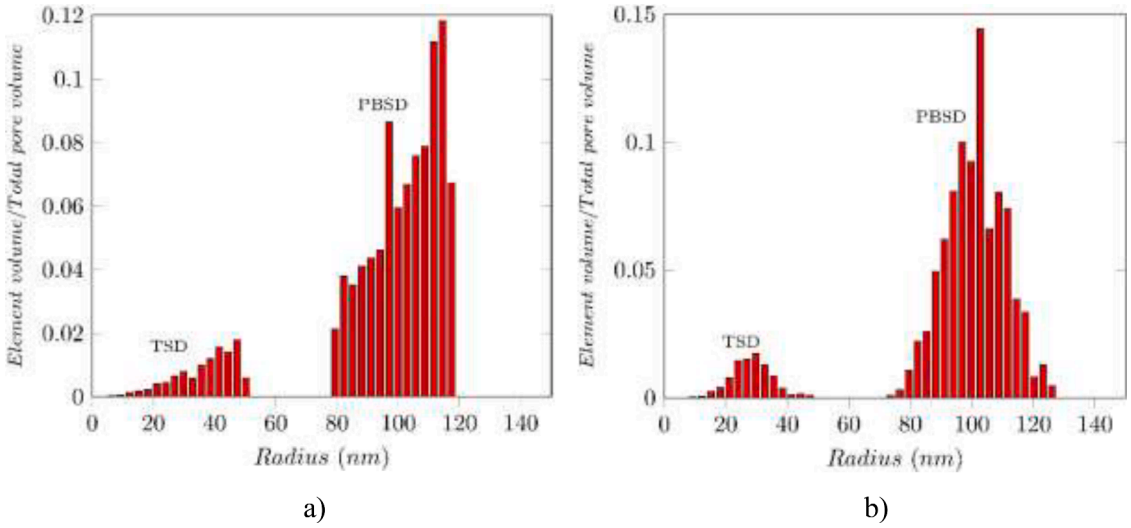


**Fig. 11.** Reference uniform (a) and Gaussian (b) TSD and PBSD after consideration of throat and pores volumes.

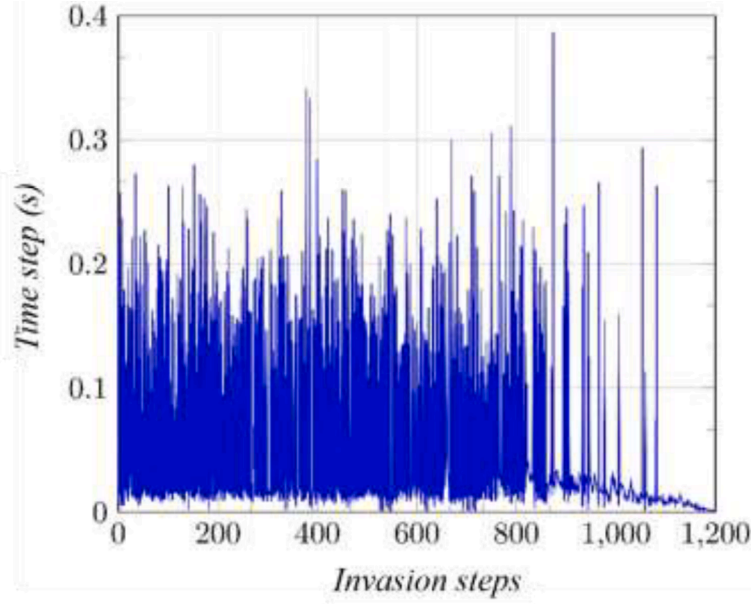


**Fig. 12.** PNM time step variation along the EP PNM simulation (Gaussian case). An invasion step corresponds to the full drying of an element, pore body or throat, in the network.

are identical to the reference ones (shown in Fig. 11b) and thus identical to the ones obtained when the PNM variable time step is used (shown in Fig. 13a). By contrast, as illustrated in Fig. 13d, the procedure leads to poor results when $\Delta t$ is set to a too large value compared to the "intrinsic" time steps characterizing the successive pore and throat invasion by the gas phase in the network. The impact is quite noticeable as regards the TSD, which is quite different from the reference TSD in Fig. 13d with identified throat sizes not present in the network while many others are missing. Also, the distribution of the larger sizes, corresponding to pore bodies, is truncated with a quite significant shift of the distribution toward smaller sizes compared to the reference distribution. For the tested intermediate time step, *i.e.,* $\Delta t$=0.1 s, the EP procedure leads to the parasitic spreading of the distribution between the TSD and the PBSD and the net separation between the TSD and PBSD is lost (Fig. 13c). As can be observed from the comparison between Figs 13a (which corresponds to the reference TSD and PBSD) and 13c ($\Delta t$ = 0.1 s), the pore size repartition between the TSD and the PBSD is significantly altered. When the time step is too large, the computation of the evaporation rate from the mass tends to smooth out the evaporation rate fluctuations. Thus, the greater the time step, $\Delta t$, compared to the intrinsic time step, the greater the loss of information on the evaporation rate. In particular, when the sampling period of the mass evolution is increased, high-frequency fluctuations are filtered out. Since these high-frequency events are a signature of larger pores emptying due to the fact that the evaporation rate increases with the pore size, it explains why the fraction of the larger pore bodies is truncated when $\Delta t$ is too large. This is illustrated in Fig. 13d which shows that the distribution obtained for $\Delta t$=1 s is even more different from the reference distribution depicted in Fig. 11b than for $\Delta t$=0.1 s.

In the experimental work on EP reported in (Krantz et al., 2013), the evaporation rate data were averaged over seven successive measurements and the result was assigned to the time at the midpoint of the corresponding interval. From the above results, it is expected that such an averaging procedure might have an impact on the resulting PBTSD because, again, it leads to a further smoothing effect of the evaporation rate fluctuations. In order to get some insight on the impact of averaging,

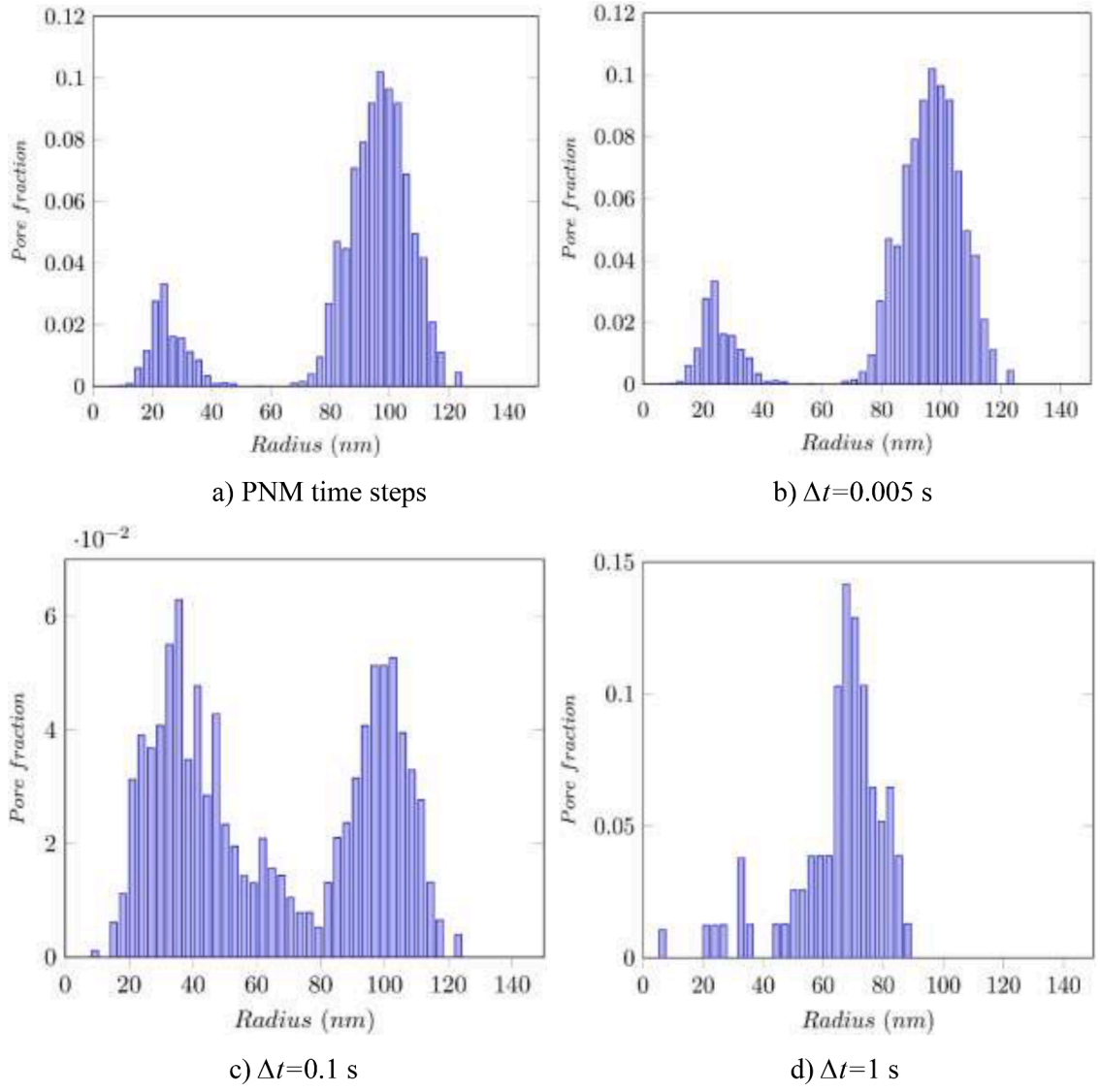


**Fig. 13.** PBTSD obtained from EP using the mass and evaporation rate computed at a varying frequency (*i.e.*, at each time step of the PNM algorithm) (a), and at fixed frequencies ($\Delta t$ = 0.005 s (b), $\Delta t$ = 0.1 s (c) and $\Delta t$ = 1 s (d)) for the reference Gaussian distributions.

the Gaussian network was considered and the evaporation rate values, obtained with a time-sampling of the mass evolution $\Delta t$=0.1 s, were averaged as indicated above. The resulting PBTSD is represented in Fig. 14. The distribution is very different from the reference one (depicted in Fig. 11b) and further altered compared to the one reported in Fig. 13c obtained without the averaging procedure. Naturally, if the time-sampling of the mass evolution is sufficiently small, then this averaging procedure does not introduce noticeable errors.

Tests were performed with the reference network featuring uniform distributions, leading to the same type of results. The averaging procedure can have a detrimental impact on the PBTSD extraction, consistently with the fact that the use of the evaporation rate computed from *m(t)* measured at a constant frequency, that is not high enough, introduces significant bias in this identification.

Additional comparison between the targets, *i.e.*, the reference TSD or PBSD, and the distributions extracted from the EP techniques is presented in Table 3. This comparison quantitatively confirms the previous results. The EP method leads to satisfactory results but is highly dependent on the accuracy with which the evaporation rate is determined. The results can be badly in error when the evaporation rate is too crudely estimated as a result of a too low measurement time frequency or an ill-adapted averaging procedure of the mass evolution. In this respect, it can be noted that the weight is recorded every 10 s in the experimental works, (Akhondi et al. 2015), (Krantz et al. 2013), (Tanis-Kanbur et al. 2019a,b). Considering, for simplicity, a cubic pore of size $d$ equal to the average pore diameter reported in Krantz *et al.* (2013), namely 98 nm, a simple estimate of a pore evaporation characteristic time can be computed from the expression $t_p = \frac{\rho d^3}{jd^2}$, where $j$ is the evaporation flux that can be deduced from the plateau evaporation rate (see Fig. 4 in Krantz *et al.* (2013)). This gives $t_p \approx 4\ s$, which is on the same order of magnitude but lower than the weight recording time (10 s). From the above discussion, this suggests that it would have been desirable to consider a shorter weight recording time in the experiments reported in this reference. These estimates also indicate that the time steps, namely $\Delta t$ = 0.005 s, $\Delta t$=0.1 s, and $\Delta t$ = 1 s, considered in relation with our simulations, should not be regarded as indicative values in the experiments. The important point illustrated by our simulations is that the weight recording time should be consistent with the mean evaporation time of a pore. Also, since $j \propto H^{-1}$, it can be seen that $t_p \propto d\ H$. Thus, the weight recording time must be specified depending on the expected pore sizes and the cell height but does not depend on the lateral extension of the porous medium, i.e. the cell diameter (Fig. 1).

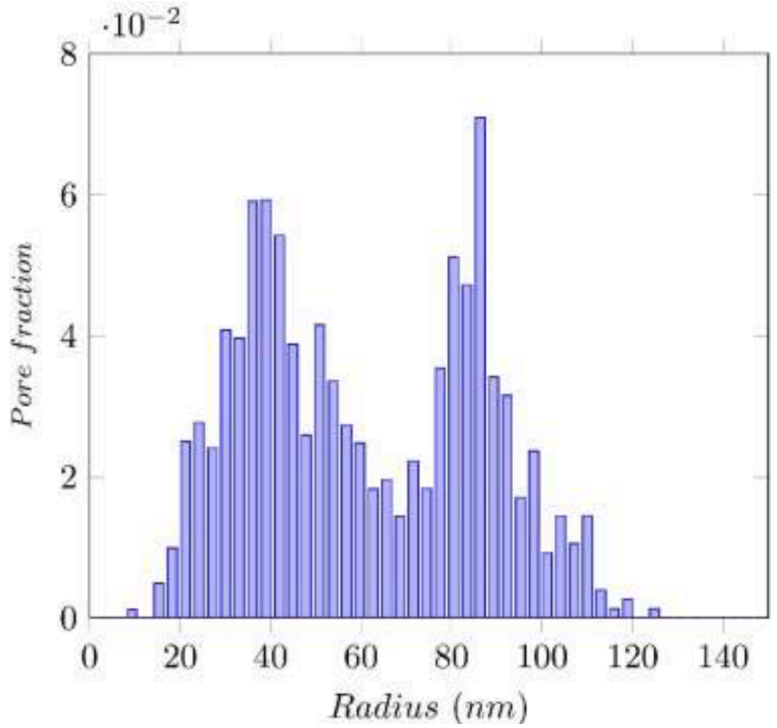


**Fig. 14.** PBTSD obtained from EP using the mass and evaporation rate computed at a fixed frequency ($\Delta t$=1 s) after averaging the evaporation rate data over seven successive values. Network with Gaussian distributions.

**Table 3**
Comparison of statistical moments (mean and standard deviation) of the reference distributions (depicted in Fig. 11) and those extracted from the EP technique. PBTSD refers to the whole element distribution, lumping the pore body and throat size distributions.

| Technique | Reference PBTSD (nm) | Extracted PBTSD (nm) | Relative error (%) | Type of reference distributions |
|---|---|---|---|---|
| EP using $W_{PNM}$ | Mean:96.72<br>Stand. Dev.:<br>23.43 | 83.27<br>24.48 | 13.91<br>4.48 | Uniform |
| EP using $W_{PNM}$ | Mean:95.77<br>Stand. Dev.:<br>23.2 | 88.22<br>26.56 | 7.89<br>14.5 | Gaussian |
| EP using $W_m$ ($\Delta t$=$\Delta t_{PNM}$) | Mean:95.77<br>Stand. Dev.:<br>23.2 | 88.22<br>26.56 | 7.89<br>14.5 | Gaussian |
| EP using $W_m$ ($\Delta t$=0.005 s) | Mean:95.77<br>Stand. Dev.:<br>23.2 | 88.22<br>26.56 | 7.89<br>14.5 | Gaussian |
| EP using $W_m$ ($\Delta t$=0.1 s) | Mean: 95.77<br>Stand. Dev.:<br>23.2 | 65.76<br>32.02 | 31.34<br>38 | Gaussian |
| EP using $W_m$ ($\Delta t$=1 s) | Mean: 95.77<br>Stand. Dev.:<br>23.2 | 65.89<br>15.95 | 31.2<br>31.25 | Gaussian |
| EP using $W_m$ with seven points averag. ($\Delta t$=0.1 s) | Mean:95.77<br>Stand. Dev.:<br>23.2 | 60.78<br>25.62 | 36.54<br>10.45 | Gaussian |

## 5. Discussion

### 5.1. Comparison with LLDP

Since the Liquid-Liquid Displacement Porosimetry (LLDP) was explored in previous works (Maalal et al., 2021a, 2022) also from pore network simulations, it is interesting to compare the outcomes of both techniques. According to (Maalal et al., 2021a), a first and important difference lies in the fact that the size distribution derived from the LLDP technique essentially corresponds to the TSD because the immiscible displacements involved in the LLDP is mainly controlled by the pore space constrictions, *i.e.*, the throats. This is in contrast with the EP technique since our simulations indicate that both the TSD and PSB can be identified with the EP technique, but again, this possibility is highly dependent on the evaporation rate measurement accuracy. Sampling frequency of the mass evolution during evaporation is a key parameter and simulation results presented here indicate that this frequency must be as high as possible. Improvement may be achieved by devising experiments featuring slow evaporation with an appropriate probing evaporating liquid having a small enough saturation vapor pressure.

In the work reported in (Tanis-Kambur et al., 2019a), the LLDP and EP techniques were compared on the basis of experiments performed on the same ultrafiltration membranes. The main results are somewhat disturbing since both techniques led to significantly different PBTSD. In this respect, together with the works presented in (Maalal et al., 2022), the present study confirms this contrast. In (Maalal et al., 2022), it is shown that viscous effects can lead to the identification of unrealistic small pores with the LLPD technique, whereas such a viscous bias is not present in the EP technique (see §5.2). However, our simulations do not permit a full explanation of the observations reported in (Tanis-Kambur et al., 2019a). For instance, the average pore size in (Tanis-Kambur et al., 2019a) is sometimes greater with the LLDP compared to the EP and sometimes smaller, depending on the porous medium under consideration. In the simulations, sizes identified from the LLDP correspond to the constriction (throat) sizes. Therefore, the identified average size is necessarily smaller than the average size obtained from the EP which includes both the pore bodies and throats. Considering the viscous effects in a highly interconnected pore network even reinforces this effect which, as mentioned above, leads to the identification of unrealistic small pore throats with the LLDP (Maalal et al., 2022). However, the results of the LLDP are highly dependent on the pore space structure. The closer the structure to a system of non-interconnected cylindrical pores in parallel, the more representative should be the

TSD as the extraction procedure from LLDP relies on this model structure. Thus, the differences in the pore space structures of the various membranes characterized in (Tanis-Kanbur et al., 2019a) should partly explain the reported differences between the LLDP and the EP. It can also be noted that the porous medium porosity was severely underestimated with the LLDP. This might be a consequence of the fact that the main outcome target of the method is the TSD, which is associated with only a small fraction of the porosity. Another result reported in (Tanis-Kanbur et al., 2019a), consistent with the present simulations, is that the spreading of the distribution, for a given membrane, is much wider with the EP than with the LLDP. This can be again partly explained by the fact that the interpretation of the EP experimental data allows determining both the throats and pore bodies sizes, but is sensitive to the evaporation rate extracted from the mass evolution record. As shown in Sect.4, the lack of accuracy on the evaporation rate tends to (wrongly) amplify the spreading of the identified distribution.

### 5.2. On the EP simulation

Simulations reported here were performed on a rather small 2D network containing 400 pore bodies (and about 800 throats). In the EP set-up used in (Tanis-Kanbur et al., 2019a), the porous medium diameter in the test cell is 35 mm and the porous medium active thickness is on the order of 10 μm. Considering that the mean distance between pore bodies is on the order of the mean pore diameters reported in (Tanis--Kanbur et al., 2019a), for example 100 nm, and assuming an isotropic pore structure, yields about 350 000 pore bodies over a porous medium diameter and 100 pore bodies over the porous medium thickness. The number of pore bodies in the real membranes is therefore several orders of magnitude larger than in the network used in this work. However, the number of pore bodies over the thickness is on the same order of magnitude (20 for the PNM against ~100 for the real membranes). Nevertheless, it would be interesting to perform simulations over larger and 3D networks in order to explore whether the small size of the network is really an issue. Also, a structured network was considered for simplicity. However, the used drying algorithm with Kelvin effect on a network is generic and can be applied to unstructured networks as well. Therefore, quite similar results are expected with unstructured networks since the drying algorithm is not specific to structured networks. Nevertheless, it would be interesting to perform simulations on unstructured networks as well. Other concerns lie in the physics of drying. In the simulations reported here, viscous effects in the liquid phase were ignored. The evaporation rate, $W$, in the EP characterization reported in (Tanis-Kanbur et al., 2019a) is on the order of $10^{-8}$ kg/s. For the cell test of 35 mm in diameter (thus of cross-section surface area $A$=9.6 $\times$ $10^{-4}$ $m^2$) used in this reference, this corresponds to an evaporation velocity $U_e = \frac{W}{\rho A} \approx 1.3 \times 10^{-8}$ m/s. This further leads to a capillary number, $Ca$, quantifying the viscous to capillary effect ratio, given by $Ca = \frac{\mu U_e}{\gamma} \approx 10^{-9}$, which is quite small. This indicates that capillary effects are strongly dominating the transfer process and that the assumption of negligible viscous effects in the liquid clusters is quite reasonable. As discussed in (Maalal et al., 2021b), another pertaining question deals with liquid films (Eijkel et al., 2005; Chauvet et al., 2009; Prat, 2007), which were ignored in the present PNM of evaporation with Kelvin effect. In the current state of the art, it is unclear whether liquid films would indeed affect the main results obtained from the PNM simulations. Incorporating the liquid films in the model in conjunction with the Kelvin effect is a tricky task, a priori, but would certainly deserve to be addressed in the future. Liquid films considered in Eijkel et al., 2005; Chauvet et al., 2009; Prat, 2007) are referred to as thick films, or capillary films, because their dynamics depends on capillary effects. In addition, adsorbed thin liquid films at the pore wall are likely to be present. Their presence may affect the pore size identification, in particular for smaller pores, when the pore opening is not large compared to the film thickness. The meniscus radius of curvature would then approximately correspond to the pore opening minus twice the film thickness and not simply to the pore opening (Takei et al., 1997). This corresponds to pores on the order of a few nm. However, this effect is not such as to question the main results of the present study.

Simulations reported above indicate a non-monotonous variation of the evaporation rate. This means that the evaporation rate can slightly increase compared to its value at a previous time. This is a direct consequence of the Kelvin effect inducing fluctuations of the menisci radii of curvature at the boundary of the liquid clusters forming during the drying process. It would be interesting to confirm this effect from dedicated experiments.

## 6. Conclusions

Evapoporometry (EP) is a technique aiming at measuring pore size distributions up to a few hundreds of nanometers. This upper bound is imposed by the sensitivity of the equilibrium vapor pressure to the meniscus curvature via the Kelvin relationship for usual volatile liquids. In this study, the EP technique was analyzed on the basis of numerical simulations in a perfectly known model pore space structure, aiming at reproducing the evaporation process at the heart of the EP technique. For the model pore space structure under consideration, the EP technique leads to quite satisfactory results. The pore body and throat size distributions can be identified and the main distribution properties are quite well retrieved. However, the quality of the results is highly dependent on the accuracy with which the evaporation rate is determined. Relatively small errors on the evaporation rate can significantly affect the results. This can lead to an erroneous identification of non-existing pore body or throat sizes and / or to an unrealistic spreading of the size distribution. In spite of the care taken in measuring the mass in the EP set-ups, (Krantz et al., 2013; Tanis-Kanbur et al., 2019a,b), it is not obvious that the level of accuracy on the determination of the evaporation rate is sufficient. The technique thus would deserve further investigation. Results extracted from EP data can be seriously in error depending on the accuracy with which the evaporation rate is determined. Yet, this study relies on numerical simulations based on assumptions to model the physical processes at play in the EP techniques and simulations were performed on a rather small two-dimensional network. In this respect, it would be interesting to perform simulations in larger networks and in three-dimensions so as to explore further the interesting capabilities of the EP technique. Nevertheless, in spite of its limitations, the present work is expected to help clarify the underlying physics at play in the EP technique.

## CRediT authorship contribution statement

**Otman Maalal:** Investigation, Software, Writing – original draft. **Marc Prat:** Conceptualization, Funding acquisition, Supervision, Writing – review & editing. **Didier Lasseux:** Conceptualization, Supervision, Writing – review & editing.

## Declaration of Competing Interest

The authors declare that they have no known competing financial interests or personal relationships that could have appeared to influence the work reported in this paper.

## Acknowledgements

This research was supported by the Project “PEMFC – SUDOE” – SOE1/P1/E0293 which is co-financed by the European Regional Development Fund in the framework of the Interreg Sudoe programme.

## References


Akhondi, E., Zamani, F., Chew, J.W., Krantz, W.B., Fane, A.G., 2015. Improved design and protocol for evapoporometry determination of the pore-size distribution. J. Membr. Sci. 496, 334–343.

Blunt, M.J., 2001. Flow in porous media-pore-network models and multiphase flow. Curr. Opin. Colloid Interface Sci. 6, 197–207.

Blunt, M.J., Jackson, M.D., Piri, M., Valvatne, P.H., 2002. Detailed physics, predictive capabilities and macroscopic consequences for pore-network models of multiphase flow. Adv. Water Res. 25 (8-12), 1069–1089.

Calvo, J.I., Peinador, R.I., Prádanos, P., Bottino, A., Comite, A., Firpo, R., Hernández, A., 2015. Porosimetric characterization of polysulfone ultrafiltration membranes by image analysis and liquid–liquid displacement technique. Desalination 357, 84–92.

Chauvet, F., Duru, P., Geoffroy, S., Prat, M., 2009. Three periods of drying of a single square capillary tube. Phys. Rev. Lett. 103, 124502.

Eijkel, J.C.T., Dan, B., Reemeijer, H.W., Hermes, D.C., Bomer, J.G., van den Berg, A., 2005. Strongly accelerated and humidity independent drying of nanochannels induced by sharp corners. Phys. Rev. Lett. 95, 256107.

Krantz, W.B., Greenberg, A.R., Kujundzic, E., Yeo, A., Hosseini, S.S., 2013. Evapoporometry: A novel technique for determining the pore-size distribution of membranes. J. Membr. Sci. 438, 153–166.

Maalal, O., Prat, M., Peinador, R., Lasseux, D., 2021a. Determination of the throat size distribution of a porous medium as an inverse optimization problem combining pore network modeling and genetic and hill climbing algorithms. Phys. Rev. E 103, 023303.

Maalal, O., Prat, M., Lasseux, D., 2021b. Pore network model of drying with Kelvin effect. Phys. Fluids 33 (2), 027103.

Maalal, O., Prat, M., Peinador, R., Lasseux, D., 2022. Evaluation of pore size distribution via fluid-fluid displacement porosimetry: the viscous bias. Int. J. Multiphase Flow 149, 103983.

Mitropoulos, A.C., 2008. The Kelvin equation. J Colloid Interface Sci 317, 643–648.

Morison, K.R., 2008. A comparison of liquid-liquid porosimetry equations for evaluation of pore size distribution. J. Membr. Sci. 325, 301–310.

Mourhatch, R., Tsotsis, T.T., Sahimi, M., 2011. Determination of the true pore size distribution by flow permporometry experiments: An invasion percolation model. J. Membr. Sci. 367, 55–62.

Peinador, R.I., Calvo, J.I., Prádanos, P., Palacio, L., Hernández, A., 2010. Characterization of polymeric UF membranes by liquid-liquid displacement porosimetry. J. Membr. Sci. 348, 238–244.

Prat, M., 1993. Percolation model of drying under isothermal conditions in porous media. Int. J. Multiphase Flow 19 (4), 691–704.

Prat, M., 2007. On the influence of pore shape, contact angle and film flows on drying of capillary porous media. Int. J. Heat Mass Transf. 50, 1455–1468.

Takei, T., Chikazawa, M., Kanazawa, T., 1997. Validity of the Kelvin equation in estimation of small pore size by nitrogen adsorption. Colloid. Polym. Sci. 275, 1156–1161.

Tanis-Kanbur, M.B., Peinador, R.I., Hu, X., Calvo, J.I., Chew, J.W., 2019a. Membrane characterization via evapoporometry (EP) and liquid-liquid displacement porosimetry (LLDP) techniques. J. Membr. Sci. 586, 248–258.

Tanis-Kanbur, M.B., Zamanic, F., Krantz, W.B., Hu, X., Chew, J.W, 2019b. Adaptation of evapoporometry (EP) to characterize the continuous pores and interpore connectivity in polymeric membranes. J. Membr. Sci. 575 (1), 17–27.

Wilkinson, D., Willemsen, J.F., 1983. Invasion percolation: a new form of percolation theory. J. Phys. A Math. Gen. 16, 3365–3376.

Zamani, F., Jayaraman, P., Akhondi, E., Krantz, W.B., Fane, A.G., Chew, J.W., 2017. Extending the uppermost pore diameter measureable via Evapoporometry. J. Membr. Sci. 524, 637–643.